










RESEARCH ARTICLE | AUGUST 22 2023

## Laser writing of parabolic micromirrors with a high numerical aperture for optical trapping and rotation

T. Plaskocinski ; Y. Arita ; G. D. Bruce ; S. Persheyev ; K. Dholakia ; A. Di Falco  ; H. Ohadi  



*Appl. Phys. Lett.* 123, 081106 (2023)

<https://doi.org/10.1063/5.0155512>



View  
Online



Export  
Citation

CrossMark

### Articles You May Be Interested In

Optimized micromirror arrays for adaptive optics

*AIP Conference Proceedings* (January 1999)



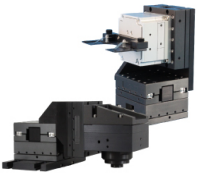
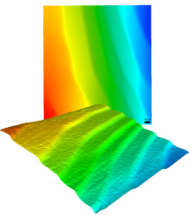
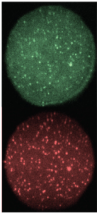
Fabrication of out-of-plane micromirrors in silicon-on-insulator planar waveguides

*Journal of Vacuum Science & Technology A* (May 2006)

High reflectivity micromirrors fabricated by coating high aspect ratio Si sidewalls

*Journal of Vacuum Science & Technology B: Microelectronics and Nanometer Structures Processing, Measurement, and Phenomena* (November 1997)

28 August 2023 13:15:30

 <p>MAD CITY LABS INC. www.madcitylabs.com</p>	<p>Nanopositioning Systems</p> 	<p>Modular Motion Control</p> 	<p>AFM and NSOM Instruments</p> 	<p>Single Molecule Microscopes</p> 
---	--	--	---	--

# Laser writing of parabolic micromirrors with a high numerical aperture for optical trapping and rotation

Cite as: Appl. Phys. Lett. **123**, 081106 (2023); doi: 10.1063/5.0155512

Submitted: 9 May 2023 · Accepted: 3 August 2023 ·

Published Online: 22 August 2023



View Online



Export Citation



CrossMark

T. Plaskocinski,<sup>1</sup> Y. Arita,<sup>1</sup> G. D. Bruce,<sup>1</sup> S. Persheyev,<sup>1</sup> K. Dholakia,<sup>1,2,3</sup> A. Di Falco,<sup>1,a)</sup> and H. Ohadi<sup>1,a)</sup>

## AFFILIATIONS

<sup>1</sup>SUPA, School of Physics and Astronomy, University of St. Andrews, North Haugh, St. Andrews, Fife KY16 9SS, United Kingdom

<sup>2</sup>School of Biological Sciences, University of Adelaide, Adelaide SA 5005, Australia

<sup>3</sup>Centre of Light for Life, University of Adelaide, Adelaide SA 5005, Australia

<sup>a)</sup> Authors to whom correspondence should be addressed: [adf10@st-andrews.ac.uk](mailto:adf10@st-andrews.ac.uk) and [ho35@st-andrews.ac.uk](mailto:ho35@st-andrews.ac.uk)

## ABSTRACT

On-chip optical trapping systems allow for high scalability and lower the barrier to access. Systems capable of trapping multiple particles typically come with high cost and complexity. Here, we present a technique for making parabolic mirrors with micrometer-size dimensions and high numerical apertures ( $NA > 1$ ). Over 350 mirrors are made by simple  $\text{CO}_2$  laser ablation of glass followed by gold deposition. We fabricate mirrors of arbitrary diameter and depth at a high throughput rate by carefully controlling the ablation parameters. We use the micromirrors for three-dimensional optical trapping of microbeads in solution, achieving a maximum optical trap stiffness of  $52 \text{ pN}/\mu\text{m}/\text{W}$ . We, then, further demonstrate the viability of the mirrors as *in situ* optical elements through the rotation of a vaterite particle using reflected circularly polarized light. The method used allows for rapid and highly customizable fabrication of dense optical arrays.

© 2023 Author(s). All article content, except where otherwise noted, is licensed under a Creative Commons Attribution (CC BY) license (<http://creativecommons.org/licenses/by/4.0/>). <https://doi.org/10.1063/5.0155512>

There has been a great interest<sup>1,2</sup> in developing optical lab-on-a-chip platforms in recent years as they are portable, robust, and scalable. Integrating multiple optical components has allowed great leaps in analyzing and sensing biological specimens.<sup>3–5</sup> One such powerful technique is optical trapping, which allows for the 3D manipulation of objects by using the transfer of momentum of light.<sup>6</sup> As a well-established technique, it has found uses in single-molecule force spectroscopy,<sup>7,8</sup> particle sorting,<sup>9,10</sup> and sensing in both the far and near field.<sup>11</sup> An optical trap is characterized by the trap stiffness  $k$ , assuming that the trapped particle is in a harmonic motion.<sup>12</sup> Furthermore, it is possible to transfer the angular momentum of light to anisotropic particles through external or internal birefringence, inducing rotation when trapped by a circularly polarized beam.<sup>13,14</sup>

The system must meet several requirements to allow for the confinement of the subject specimen in an optical potential in the far field: the particle must be of a higher refractive index than the surrounding medium and, for optimal performance, should be of a size comparable to that of the wavelength of the trapping beam.<sup>15,16</sup> In addition, a tightly focused beam is necessary to provide a large enough restoring force for trapping. A bulky, high numerical aperture (NA) and high

magnification microscope objective is required, with multiple drawbacks. For one, the objective size makes the integration difficult, and the high magnification brings a small field of view, limiting the number of simultaneously manipulated samples. These and the high cost of high-NA objectives have resulted in the poor integration and scalability of the optical trapping platform.

Multiple schemes have been developed in the last two decades to address these issues to enable on-chip trapping.<sup>17</sup> These include creating an optical lattice through interference,<sup>9</sup> near and far field trapping enabled by fibers,<sup>18</sup> as well as working to replace the microscope objective with a high numerical aperture but a much smaller optical lens equivalent, capable of similar focusing performance. The best performing have been metasurfaces,<sup>19</sup> placed at the bottom of the microfluidic chamber for trapping in reflection,<sup>19,20</sup> grafted on top for trapping in transmission<sup>21</sup> or placed on tips of optical fibers.<sup>22</sup> With NA ranging from 0.56 to 1.2,<sup>19,23</sup> they can reach a performance almost matching that of high NA objectives, all while keeping a small footprint on the order of a square millimeter. Another option is the Fresnel diffractive elements.<sup>24–26</sup> However, for both systems, the fabrication process is time-consuming and expensive. Additionally, the small and delicate

optical elements, which make up these lenses, can be easily damaged. Depending on the geometry, they will be wavelength-specific and polarization sensitive. Microlenses and micromirrors,<sup>27,28</sup> however, do not suffer from these problems. By imprinting pre-made lenses,<sup>29,30</sup> arrays of traps with relatively high NA have been fabricated. While convenient, this method is limited by the variety of lenses available to consumers. Chemical treatment can also be combined with other techniques to etch smooth mirrors into the substrate.<sup>31–34</sup> A method often combined with etching is silica CO<sub>2</sub> laser ablation, a well-established glass treatment process whereby a short ( $\sim 100$  ns) pulse is used to form an approximately hemispherical mirror.<sup>35</sup> Silica is exceptionally absorbent for radiation above  $4\ \mu\text{m}$ ,<sup>36</sup> meaning that a focused beam of CO<sub>2</sub> laser with a wavelength of  $10.6\ \mu\text{m}$  can evaporate the glass directly at the focus, melting the glass around it. The vapor pressure from the evaporation then creates a melt front, which travels away from the center until the glass re-solidifies, the entire process occurring in under a second.<sup>37,38</sup>

Here, we present a significantly faster, more customizable technique for creating trapping arrays with high numerical aperture. Using a continuous wave (CW) CO<sub>2</sub> laser, we write micromirror structures through ablation. First, we expose the glass substrate for  $\sim 100$  ms to a focused TEM<sub>00</sub> mode of the laser, resulting in a nearly parabolic mirror profile.<sup>39</sup> The glass is then coated with a thin gold layer to achieve a smooth reflective surface. We show that by tuning the ablation parameters, the diameter and depth of the micromirrors can be controlled accurately based on the required application. To demonstrate the platform's viability, we use a high NA micromirror to trap  $5\ \mu\text{m}$  vaterite and  $2\ \mu\text{m}$  silica particles suspended in D<sub>2</sub>O. As shown in Fig. 1, we use a hybrid optical setup that interchangeably allows trapping by a high NA objective or micromirrors. While not necessary to enable trapping, it is convenient for this demonstration, as trapping can be performed passively by illuminating using a collimated beam. We characterize the optical performance of the mirror and then proceed to use it to reverse the direction of rotation of a vaterite particle. Through this, we demonstrate the potential of micromirrors as a simple-to-fabricate and versatile lab-on-chip optical platform.

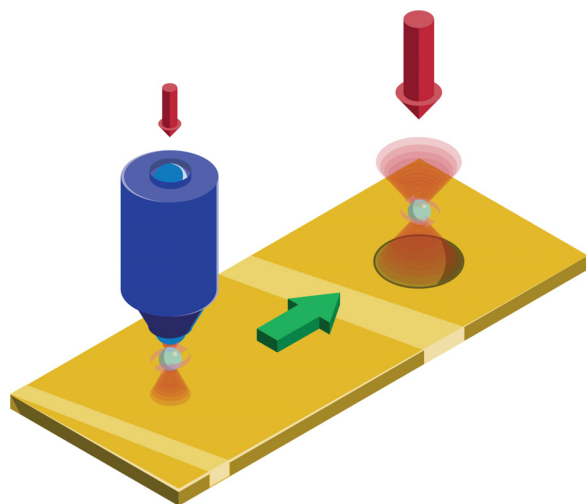


**FIG. 1.** The optical trapping platform schematic. Traditional optical tweezers (left) are used to deliver a bead to micromirror-enabled optical tweezers (right).

At the core of the setup for the fabrication of the micromirrors is the CO<sub>2</sub> ablation laser (Synrad 48-KA CW 25 W) [see Fig. 2(a)]. We controlled the duration of the ablation using a mechanical shutter (Thorlabs SC10) and set the average power through the duty cycle of the laser ( $\sim 8\%$ , corresponding to  $\sim 1.2$  W at the sample plane). The glass sample was mounted vertically on a motorized 3D stage (Newport, Picomotor actuators). A visible diode laser ( $\lambda_D = 660$  nm) with an adjustable divergence was used as a guide to precisely locate the  $x$ ,  $y$ , and  $z$  positions of the focused CO<sub>2</sub> laser beam on the sample. For monitoring, we used a CMOS camera (Thorlabs DCC1545M) in conjunction with a collimated light-emitting diode. The shutter, CO<sub>2</sub> laser, and stage were synchronized and controlled using LabVIEW to rapidly fabricate customized arrays of micromirrors, as shown in Fig. S1. The automation also allowed for writing continuous channels in glass, as shown in Fig. S2. The beam profile of the CO<sub>2</sub> laser was spatially filtered using an aperture and finally focused onto the glass sample to a size of  $\sim 100\ \mu\text{m}$  using a ZnSe plano-convex lens ( $f = 15$  mm), which also served as the imaging lens for the camera. After ablation, the sample was transferred to an electron beam evaporator (Edwards

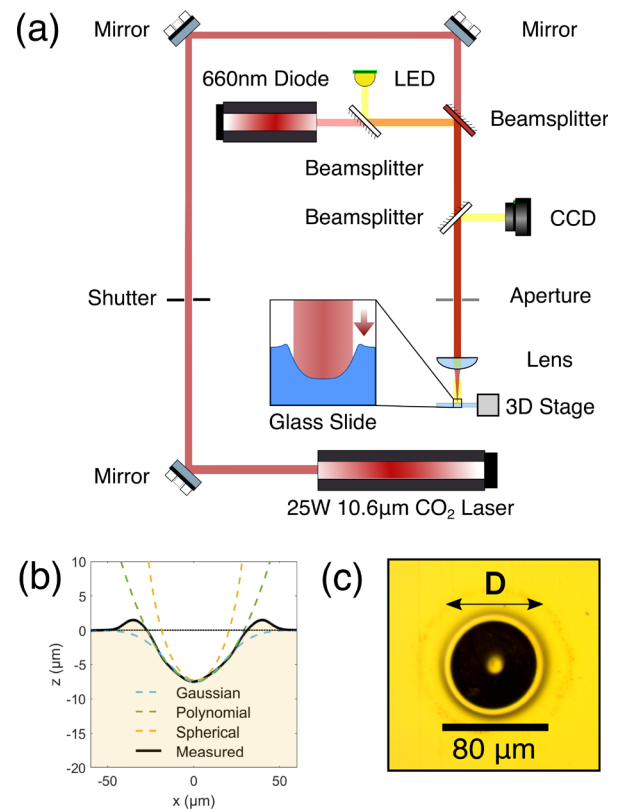


**FIG. 2.** (a) Setup used in micromirror fabrication, with automated shutter, laser, and 3D stage. The lenses and beam splitters for the CO<sub>2</sub> laser were ZnSe-coated to minimize loss. (b) Top-down view of a gold-coated micromirror with diameter  $D = 80\ \mu\text{m}$ . The bright spot in the center is the reflection of the illuminating lamp. (c) Gaussian, spherical, and polynomial fitting of the mirror profile fabricated with laser power of  $1.8$  W, single pulse time of  $\tau = 120$  ms, and aperture diameter of  $2$  mm. We used this mirror for both the trapping and rotation of particles. Refer to Table I for all parameters.

AUTO 306), where a 2 nm thick adhesion layer of NiCr was deposited, followed by 150 nm of gold. We characterized the micromirrors using optical microscopy and a surface profiler. We used optical microscopy to extract the mirror diameter and depth [Fig. 2(b)] and a contact mode profilometer (Veeco Dektak 150 with a 12  $\mu\text{m}$  stylus) to accurately map the profile [Fig. 2(c)]. The figure shows the micromirror used for particle trapping with depth  $z = 7.3 \mu\text{m}$  and diameter  $D = 56.5 \mu\text{m}$ . The mirror profile resembles the Gaussian intensity profile of the CO<sub>2</sub> beam with deviations due to the long pulse durations used, meaning that a parabola more accurately describes the profile.<sup>37</sup> The exact scan geometry and alternative view of the profile are shown in Fig. S3. In total, 357 micromirrors with diameters of  $\sim 40$ – $120 \mu\text{m}$  were fabricated and characterized. We considered five parameters: the laser power, the position of the focus relative to the substrate, the duration and the number of exposures, and the size of the aperture [shown in Fig. 2(a)]. We found that the final profile of the micromirror was relatively insensitive to the duration and number of exposures, indicating that the shortest exposure created by the shutter ( $\sim 50$  ms) was longer than the ablation timescale. In addition, the diameter of the micromirrors initially displayed a simple linear relationship with the laser power, which plateaued as the mirrors' diameter approached that of the focused beam. Finally, the depth of the micromirrors reached an upper bound at higher laser power ( $\sim 2$  W), where the rapid change in temperature gradient resulted in cracks forming at the bottom of the mirrors. Furthermore, the diameter and the depth of the micromirrors had a nearly linear dependence on the aperture diameter. The exact position of the focus had the most substantial effect on the micromirror profile. If the mirror's center evaporated too quickly, it formed a secondary curvature inside the first, as the melt front would not move fast enough. Hence, the beginning of each fabrication included a calibration step where the exact  $z$ -plane was chosen based on the mirror shape observed through the CCD after ablation. For further information on mirror ablation, see the supplementary material Figs. S4–S7.

To translate the measurable mirror diameter and depth into a usable metric of NA, we used a geometric approximation following profile measurements, which clearly showed a parabolic profile of the mirror, as seen in Fig. 2(c). The focal length  $f$  of the parabola is<sup>40</sup>

$$f = \frac{D^2}{16z}, \quad (1)$$

where  $D$  is the mirror diameter, and  $z$  is the depth. We define the aperture angle  $\theta$  of a parabolic mirror as

$$\frac{z}{f} = \frac{D^2}{16f^2} = \tan^2\left(\frac{\theta}{2}\right). \quad (2)$$

We clearly show the relationship between  $z/D$  and  $\theta$  in Fig. 3(b), where the parameters of 357 mirrors are plotted according to their estimated aperture angle. Of course, this is a simple geometric approximation. Especially for higher ratios of  $D$  and  $z$ , the effects of higher fabrication power causing cracks and uneven surfaces must be considered. It is also important to note that as  $\theta$  increases over  $\pi/2$  degrees, the trapping decreases in quality as more of the light contributes to the scattering force incident on the particle. For mirrors with  $\theta < \pi/2$ , a comparison can be made to a lens, using NA as the figure of merit. Taking the relationship between NA and  $\theta$  to be  $NA = n_m \sin(\theta)$ , where  $n_m$  is the refractive index of the medium (1.33 for D<sub>2</sub>O), we can define an effective NA of the micromirrors defined as

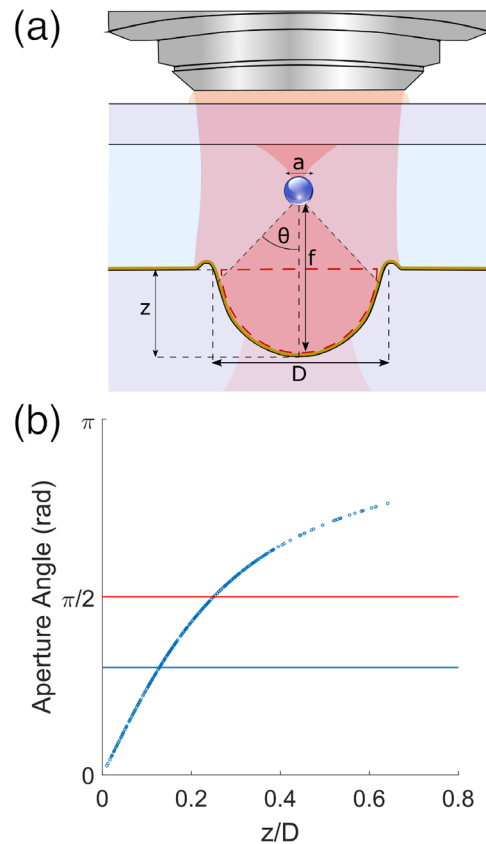


**FIG. 3.** (a) Micromirror trapping scheme, with the depth  $z$ , diameter  $D$ , focal length  $f$ , the radius of curvature  $ROC$  and aperture angle  $\theta$  as parameters of the mirror, and  $a$  is the particle size. (b) Relationship between the aperture angle  $\theta$  of the micromirrors and the depth-to-width ratio ( $z/D$ ). The red line is the maximum possible angle before focusing inside the mirror, corresponding to an NA of 1.33 in D<sub>2</sub>O. The blue line indicates the angle of the NA = 1.08 mirror used in the trapping experiment. Each point represents a mirror.

$$NA = n_m \sin\left(2 \tan^{-1}\left(\sqrt{\frac{16z^2}{D^2}}\right)\right). \quad (3)$$

It is important to note that this comparison with lenses is only valid for mirrors where  $\theta \leq \pi/2$ , whereas for an infinitely extending parabolic mirror,  $\theta$  approaches  $\pi$ .

The hybrid setup used for trapping and rotating the particles is shown in Fig. 4. The trapping laser (Omicron LuXx) had a total power of 230 mW at 830 nm and was linearly polarized (Thorlabs LPNIRB050), after which the beam was expanded by ten times using a telescope. The laser beam could then follow one of two paths depending on whether trapping by the objective (path 1) or micromirrors (path 2) was required. Path 1 (marked in blue in Fig. 4) uses a half-wave plate to match the beam's polarization to that of a spatial light modulator (SLM, Meadowlark 1920  $\times$  1152) for moving the tweezers. The beam was, then, sent through a 4*f* system conjugating the plane of the SLM and the back focal plane of an inverted water immersion objective (Olympus UPLANSAPO, 60 $\times$ , NA = 1.2). The use of the SLM was not necessary but allowed for the convenient alignment of

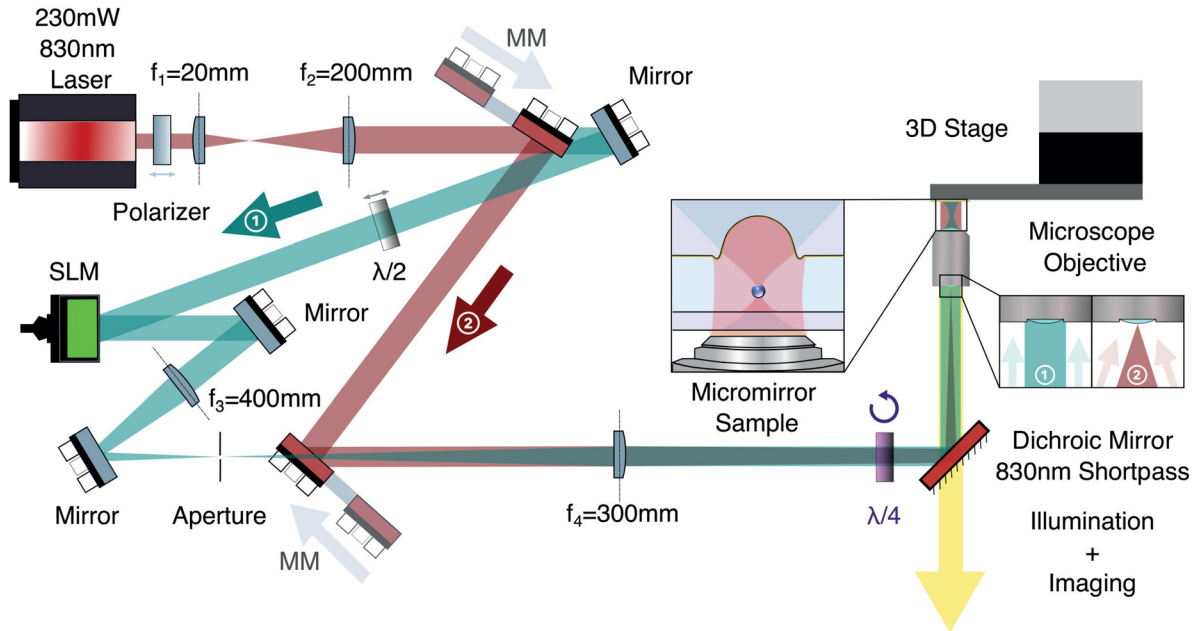


**FIG. 4.** Hybrid optical setup used for trapping particles with the standard optical tweezers using a microscope objective (path 1, blue) and micromirrors (path 2, red). The switching between paths is enabled by using movable mirrors (MMs).

the particle and mirror illumination when switching paths. For the rotation of particles, the beam was circularly polarized using a quarter-wave plate to allow for the transfer of angular momentum to birefringent particles. Path 2 (marked in red) could be switched using a pair of mirrors placed on a motorized linear stage (Thorlabs ELL20). The beam was then focused onto the back of the microscope objective (Fourier plane) using a lens ( $f_4 = 300$  mm) and the quarter-wave plate for circular polarization. In this way, the incident beam onto the micromirrors would be collimated and circularly polarized. The illumination consisted of a fiber-coupled LED, and the imaging used a CCD camera (Basler acA640–750um) with an 800 nm short-pass filter in front of it.

The microfluidic chamber containing the mirrors and particles was prepared by placing a 100  $\mu\text{m}$  thick vinyl spacer with a hole in the middle to create a well around the mirrors, then depositing the solution of particles, placing a coverslip on top and sealing the edges using nail varnish. The schematic is shown in Fig. S8. Particle loading on micromirrors consisted of first trapping a particle (either silica or vaterite) using the high-NA microscope objective (path 1), then delivering it  $\sim 5 \mu\text{m}$  below the focal point of the micromirrors. Next, path 2 was switched, resulting in a collimated beam illuminating the entire micromirror, forming the optical trap (see the supplementary material video SV1). The handover from objective to micromirror would take  $< 1$  s.

To quantify the quality of the trapping in the micromirror (see Table I for parameters), the mirror’s trap stiffness was calculated. For all trapping stiffness comparisons,  $2.02 \pm 0.015 \mu\text{m}$  particles (Duke Standards) were used to ensure consistency. First, five videos were taken of the trapped particle at 15 different powers, each video being 10 s long and having a framerate of 1000 fps resulting in 50 000 frames containing information about the position variation of the particle for

a given power. Next, the exact  $x$  and  $y$  positions of the center of mass of the particles were extracted using a previously demonstrated scheme using the shift property of the Fourier transform to symmetrize all images and obtain their relative displacement.<sup>41</sup> A power spectrum density of the positions was then plotted and fitted with a Lorentzian to acquire a corner frequency  $f_c$ , which was then converted to a trap stiffness through<sup>12</sup>

$$k_{\text{trap}} = 2\pi \cdot \underbrace{6\pi\eta a}_{\text{Stokes relation}} \cdot f_c, \quad (4)$$

where  $\eta$  is the viscosity of  $\text{D}_2\text{O}$  (1.247 mPa s at room temperature), and  $a$  is the particle’s radius. Heavy water was used due to a lower absorption coefficient at higher wavelengths.<sup>42</sup> No proximity correction was necessary as the particle was situated directly in the middle of the chamber. Five stiffness values were obtained for each power, then averaged and plotted against the power measured after the microscope objective [see Fig. 5(a)]. The dashed line is a straight-line fit with no intercept, which yielded a stiffness  $k_{\perp} = (52 \pm 1) \text{ pN}/\mu\text{m}/\text{W}$ , when correcting for the size of the beam incident on the mirror (see Fig. S9). The value is nearly six times lower than that of the objective with  $\text{NA} = 1.2$  with a stiffness of  $k_o = (332 \pm 2) \text{ pN}/\mu\text{m}/\text{W}$ . An image and diagram of the beam profile can be found in Fig. S10, showing a

**TABLE I.** Parameters of the micromirror used to trap and rotate particles. In order: diameter, depth, focal length, the ROC, effective numerical aperture, and trap stiffness of the average of  $x$  and  $y$ .

D ( $\mu\text{m}$ )	z ( $\mu\text{m}$ )	$f_m$ ( $\mu\text{m}$ )	ROC ( $\mu\text{m}$ )	NA	$k_{\perp}$ (pN/ $\mu\text{m}/\text{W}$ )
56.5	7.3	54.7	109.4	1.08	$52 \pm 1$

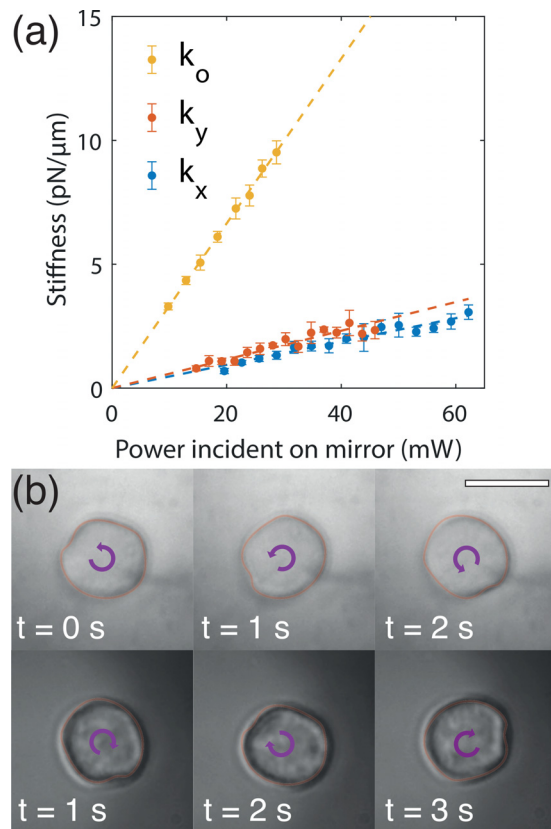


**FIG. 5.** (a) Trap stiffness of the particle in x (blue) and y (orange), and the trap stiffness of the objective with NA = 1.2 (yellow). (b) Rotation of vaterite using traditional optical tweezers (bottom) and the micromirror (top). The scale bar is 5  $\mu\text{m}$ .

FWHM of  $\sim 630$  nm. Thermal effects are an obvious concern due to the presence of gold: multiple studies have shown that a significant effect from heating is experienced by particles less than a few micrometers away from the surface, with a focused beam incident on the gold surface.<sup>43–45</sup> However, in our case, the particle is over 50  $\mu\text{m}$  above the gold surface, the beam is dispersed across an area orders of magnitude larger and combined with the linear response to changes to the laser power, thermal currents are not expected to have contributed to the trapping dynamics. Also, although the coherence length of our laser would allow for interference, given the relative intensity of the incident collimated beam and the reflective focused beam at the location of the trapping, we exclude the effects of standing waves. Given the wavelength of 830 nm resulting in fringes every 415 nm and the depth of field of our objective of  $\sim 800$  nm, we would also have seen the significant displacement of the particle in z, which is absent.

To further show the potential of our platform as a versatile alternative to a microscope objective, we demonstrated its ability to reverse the preferred direction of rotation of a  $\sim 5$   $\mu\text{m}$  piece of vaterite. While microvaterite has been shown to reach rotation speeds of up to 5 MHz in vacuum<sup>13</sup> and up to 400 Hz in water,<sup>46</sup> the rate is highly dependent on the power at the sample plane and the particle size (typically in hundreds of nanometers). In our demonstration, we place a quarter-wave plate before the objective at  $45^\circ$  with respect to the direction of

linear polarization to ensure circular polarization and verify the circularity using a polarimeter (Thorlabs PAX1000IR1) before and after the objective. We first trap the vaterite using objective-enabled optical tweezers and observe the clockwise rotation of the particle, as shown in the bottom panel of Fig. 5(b) and SV2. We then switch the optical path to trap using the micromirror and observe the particle change in the direction of rotation, as shown in the top panel of Fig. 5(b) and SV3. To simplify the trapping process, we used relatively large pieces of vaterite ( $\sim 5$   $\mu\text{m}$  diameter), which were quite asymmetric. These conditions, combined with the low power of our system ( $< 30$  mW vs typical W used<sup>47</sup>), mean that we observed the particle exhibit a preferred axis of rotation. This is clearly seen in SV2 and SV3 and manifests through a non-uniform rotation rate. We have also considered the role of the angle of reflection on the circular polarization of the reflected beam, as while the effect of reflection from a plane is understood, the case is not as clear for a curved surface, such as a parabolic mirror.<sup>48</sup> While this would be a concern for extreme angles, as can be seen in Fig. S3(b) most of the reflections from the mirror happen for  $\theta < 45^\circ$ , where significant differences between s and p components of the polarization could become apparent.

In conclusion, we describe the rapid and versatile fabrication process of 357 high-NA parabolic micromirrors with diameters in the range of 80  $\mu\text{m}$  using CW  $\text{CO}_2$  laser ablation of silica, followed by gold coating. We show that the micromirrors can be used as a substitute for microscope objectives for optical trapping. We thoroughly analyze the trapping performance at multiple powers, yielding an average stiffness of  $k_{\perp} = (52 \pm 1)$  pN/ $\mu\text{m}/\text{W}$  for a mirror with an effective NA = 1.08 comparable with values in the literature.<sup>16,49</sup> Finally, we demonstrate the ability of the mirror to counter-rotate a vaterite particle. The mirror geometry is promising in creating integrated dual-beam trapping.<sup>50</sup> As closely spaced arrays of arbitrary size can be fabricated, this scheme is a promising technique for on-chip particle trapping and sorting and optical lattices for atoms.<sup>51–53</sup> Similar schemes have also shown great promise regarding the parametric cooling of particles in vacuum.<sup>54</sup> With an added laser writing capability, we envisage that guiding particles in arbitrary circuits by 2D trapping in channels would now be feasible in this platform.

See the supplementary material for videos of particle trapping and rotation, fabrication, and characterization details.

This work was supported by the U.K. Engineering and Physical Sciences Research Council (Nos. EP/P030017/1 and EP/S014403/1) and by the European Research Council (ERC) under the European Union Horizon 2020 Research and Innovation Program (Grant Agreement No. 819346). H.O. acknowledges support from the Carnegie Trust for Universities of Scotland (Grant No. RIG007685). K.D. acknowledges support from the Australian Research Council (Grant No. DP220102303).

## AUTHOR DECLARATIONS

### Conflict of Interest

The authors have no conflicts to disclose.

### Author Contributions

**Tomasz Plaskocinski:** Data curation (equal); Formal analysis (equal); Investigation (equal); Methodology (equal); Software (equal);

Validation (equal); Visualization (equal); Writing – original draft (equal); Writing – review & editing (equal). **Yoshihiko Arita**: Conceptualization (supporting); Supervision (supporting). **Graham D. Bruce**: Supervision (supporting); Validation (supporting); Writing – review & editing (supporting). **Saydulla Persheyev**: Resources (supporting). **Kishan Dholakia**: Conceptualization (equal); Funding acquisition (equal); Resources (equal); Supervision (equal); Writing – review & editing (supporting). **Andrea Di Falco**: Funding acquisition (equal); Investigation (equal); Methodology (equal); Project administration (equal); Resources (equal); Supervision (equal); Validation (equal); Writing – review & editing (equal). **Hamid Ohadi**: Conceptualization (equal); Funding acquisition (equal); Investigation (equal); Methodology (equal); Project administration (equal); Resources (equal); Supervision (equal); Validation (equal); Writing – review & editing (equal).

## DATA AVAILABILITY

The data that support the findings of this study are openly available in the Dataset of the University of St. Andrews Research Portal at <https://doi.org/10.17630/393b6b47-cca8-40df-b2e7-81ba46fb0cfb> (Ref. 55).

## REFERENCES

- <sup>1</sup>J. M. Zhu, X. Q. Zhu, Y. F. Zuo, X. J. Hu, Y. Shi, L. Liang, and Y. Yang, *Opto-Electron. Adv.* **2**, 19000701 (2019).
- <sup>2</sup>D. Ozcelik, H. Cai, K. D. Leake, A. R. Hawkins, and H. Schmidt, *Nanophotonics* **6**, 647 (2017).
- <sup>3</sup>M. Padgett and R. Di Leonardo, *Lab Chip* **11**, 1196 (2011).
- <sup>4</sup>J. A. Huang, Y. L. Zhang, H. Ding, and H. B. Sun, *Adv. Opt. Mater.* **3**, 618 (2015).
- <sup>5</sup>S. Chen and M. H. Shamsi, *J. Micromech. Microeng.* **27**, 083001 (2017).
- <sup>6</sup>A. Ashkin, *Phys. Rev. Lett.* **24**, 156 (1970).
- <sup>7</sup>C. A. Campugan, K. R. Dunning, and K. Dholakia, *Contemp. Phys.* **61**, 277 (2020).
- <sup>8</sup>M. D. Wang, H. Yin, R. Landick, J. Gelles, and S. M. Block, *Biophys. J.* **72**, 1335 (1997).
- <sup>9</sup>M. P. MacDonald, G. C. Spalding, and K. Dholakia, *Nature* **426**, 421 (2003).
- <sup>10</sup>K. D. Leake, B. S. Phillips, T. D. Yuzvinsky, A. R. Hawkins, and H. Schmidt, *Opt. Express* **21**, 32605 (2013).
- <sup>11</sup>T. D. Bouloumis and S. N. Chormaic, *Appl. Sci.* **10**, 1375 (2020).
- <sup>12</sup>K. C. Neuman and S. M. Block, *Rev. Sci. Instrum.* **75**, 2787–2809 (2005).
- <sup>13</sup>Y. Arita, M. Mazilu, and K. Dholakia, *Nat. Commun.* **4**, 2374 (2013).
- <sup>14</sup>G. D. Bruce, P. Rodríguez-Sevilla, and K. Dholakia, *Adv. Phys.: X* **6**, 1838322 (2021).
- <sup>15</sup>N. K. Metzger, M. Mazilu, L. Kelemen, P. Ormos, and K. Dholakia, *J. Opt.* **13**, 044018 (2011).
- <sup>16</sup>A. Rohrbach, *Phys. Rev. Lett.* **95**, 168102 (2005).
- <sup>17</sup>P. Paiè, T. Zandrini, R. M. Vázquez, R. Osellame, and F. Bragheri, *Micromachines* **9**, 200 (2018).
- <sup>18</sup>Y. Lou, D. Wu, and Y. Pang, *Adv. Fiber Mater.* **1**, 83 (2019).
- <sup>19</sup>J. Xiao, T. Plaskocinski, M. Biabanifard, S. Persheyev, and A. Di Falco, *ACS Photonics* **10**, 1341 (2023).
- <sup>20</sup>G. Tkachenko, D. Stellinga, A. Ruskuc, M. Chen, K. Dholakia, and T. F. Krauss, *Opt. Lett.* **43**, 3224 (2018).
- <sup>21</sup>K. Shen, Y. Duan, P. Ju, Z. Xu, X. Chen, L. Zhang, J. Ahn, X. Ni, and T. Li, *Optica* **8**, 1359 (2021).
- <sup>22</sup>M. Plidschun, H. Ren, J. Kim, R. Förster, S. A. Maier, and M. A. Schmidt, *Light: Sci. Appl.* **10**, 57 (2021).
- <sup>23</sup>H. Markovich, I. I. Shishkin, N. Hendler, and P. Ginzburg, *Nano Lett.* **18**, 5024 (2018).
- <sup>24</sup>Y. Y. Sun, X. C. Yuan, L. S. Ong, J. Bu, S. W. Zhu, and R. Liu, *Appl. Phys. Lett.* **90**, 031107 (2007).
- <sup>25</sup>J. N. Kuo and H. Z. Hu, *Jpn. J. Appl. Phys., Part 1* **50**, 04DC20 (2011).
- <sup>26</sup>E. Schonbrun, C. Rinzier, and K. B. Crozier, *Appl. Phys. Lett.* **92**, 071112 (2008).
- <sup>27</sup>C. H. Sow, A. A. Bettiol, Y. Y. Lee, F. C. Cheong, C. T. Lim, and F. Watt, *Appl. Phys. B* **78**, 705 (2004).
- <sup>28</sup>F. Merenda, J. Rohner, and J.-M. Fournier, *Opt. Express* **15**, 6075 (2007).
- <sup>29</sup>X. Zhao, Y. Sun, J. Bu, S. Zhu, and X. C. Yuan, *Appl. Opt.* **50**, 318 (2011).
- <sup>30</sup>F. Merenda, M. Grossenbacher, S. Jeney, L. Forró, and R.-P. Salathé, *Opt. Lett.* **34**, 1063 (2009).
- <sup>31</sup>A. Matsutani, M. Sato, K. Hasebe, and A. Takada, *Sens. Mater.* **31**, 1325 (2019).
- <sup>32</sup>D. L. Kendall, G. R. de Guel, S. Guel-Sandoval, E. J. Garcia, and T. A. Allen, *Appl. Phys. Lett.* **52**, 836 (1988).
- <sup>33</sup>Z. Mokhtadir, E. Koukharenka, M. Kraft, D. M. Bagnall, H. Powell, M. Jones, and E. A. Hinds, *J. Micromech. Microeng.* **14**, S82 (2004).
- <sup>34</sup>D. Najer, M. Renggli, D. Riedel, S. Starosielec, and R. J. Warburton, *Appl. Phys. Lett.* **110**, 011101 (2017).
- <sup>35</sup>T. Ruelle, M. Poggio, and F. Braakman, *Appl. Opt.* **58**, 3784 (2019).
- <sup>36</sup>C. W. Carr, H. B. Radousky, A. M. Rubenchik, M. D. Feit, and S. G. Demos, *Phys. Rev. Lett.* **92**(8), 087401 (2004).
- <sup>37</sup>D. Hunger, C. Deutsch, R. J. Barbour, R. J. Warburton, and J. Reichel, *AIP Adv.* **2**, 012119 (2012).
- <sup>38</sup>K. M. Nowak, H. J. Baker, and D. R. Hall, *Appl. Opt.* **45**, 162 (2006).
- <sup>39</sup>D. Hunger, T. Steinmetz, Y. Colombe, C. Deutsch, T. W. Hänsch, and J. Reichel, *New J. Phys.* **12**, 065038 (2010).
- <sup>40</sup>N. Lindlein, R. Maiwald, H. Konermann, M. Sondermann, U. Peschel, and G. Leuchs, *Laser Phys.* **17**, 927 (2007).
- <sup>41</sup>I. T. Leite, S. Turtaev, X. Jiang, M. Šiler, A. Cuschieri, P. S. J. Russell, and T. Čizmar, *Nat. Photonics* **12**, 33 (2018).
- <sup>42</sup>C. L. Braun and S. N. Smirnov, *J. Chem. Educ.* **70**, 612 (1993).
- <sup>43</sup>D. Lu, F. Gámez, and P. Haro-González, *Micromachines* **12**, 954 (2021).
- <sup>44</sup>Z. Xu, W. Song, and K. B. Crozier, *ACS Photonics* **5**, 4993 (2018).
- <sup>45</sup>H. D. Wang, W. Bai, B. Zhang, B. W. Li, F. Ji, and M. C. Zhong, *Photonics* **9**, 473 (2022).
- <sup>46</sup>A. I. Bishop, T. A. Nieminen, N. R. Heckenberg, and H. Rubinsztein-Dunlop, *Phys. Rev. Lett.* **92**, 198104 (2004).
- <sup>47</sup>Y. Arita, J. M. Richards, M. Mazilu, G. C. Spalding, S. E. Skelton Spesytyeva, D. Craig, and K. Dholakia, *ACS Nano* **10**, 11505 (2016).
- <sup>48</sup>M. Mansuripur, A. R. Zakharian, and E. M. Wright, *Phys. Rev. A* **84**, 033813 (2011).
- <sup>49</sup>Y. Yang, Y. X. Ren, M. Chen, Y. Arita, and C. Rosales-Guzmán, *Adv. Photonics* **3**, 034001 (2021).
- <sup>50</sup>G. Thalhammer, R. Steiger, S. Bernet, and M. Ritsch-Marte, *J. Opt.* **14**, 044024 (2011).
- <sup>51</sup>T. N. Bandi, V. G. Minogin, and S. N. Chormaic, *Phys. Rev. A* **78**, 013410 (2008).
- <sup>52</sup>R. Mu, J. Lu, S. Xu, X. Ji, and J. Yin, *J. Opt. Soc. Am. B* **26**, 80 (2009).
- <sup>53</sup>M. Sondermann, M. Fischer, and G. Leuchs, *Adv. Quantum Technol.* **3**, 2000022 (2020).
- <sup>54</sup>J. Vovrosh, M. Rashid, D. Hempston, J. Bateman, M. Paternostro, and H. Ulbricht, *J. Opt. Soc. Am. B* **34**, 1421 (2017).
- <sup>55</sup>T. Plaskocinski, Y. Arita, G. D. Bruce, S. Persheyev, K. Dholakia, A. Di Falco, and H. Ohadi, “Laser Writing of Parabolic Micromirrors with a High Numerical Aperture for Optical Trapping and Rotation (dataset),” Dataset. University of St Andrews Research Portal. <https://doi.org/10.17630/393b6b47-cca8-40df-b2e7-81ba46fb0cfb>